Erschienen in: Dalton Transactions ; 48 (2019), 4. - S. 1171-1174
https://dx.doi.org/10.1039/C8DT04823A

Four different emissions from a Pt(Bodipy)$(PEt_3)_2$(S-Pyrene) dyad

Peter Irmler,[a] Franciska S. Gogesch,[a] Christopher B. Larsen,[b] Oliver S. Wenger [b] and Rainer F. Winter *[a]

The Pt(bodipy)-(mercaptopyrene) dyad BPtSPyr shows four different emissions: intense near-infrared phosphorescence (Φ_{ph} up to 15%) from a charge-transfer state $pyrS^{\bullet+}$-Pt-$BDP^{\bullet-}$, additional fluorescence and phosphorescence emissions from the $^1\pi\pi^*$ and $^3\pi\pi^*$ states of the bodipy ligand at r.t., and phosphorescence from the pyrene $^3\pi\pi^*$ and the bodipy $^3\pi\pi^*$ states in a glassy matrix at 77 K.

In accordance with Kasha's rule, the vast majority of compounds emits solely from their lowest excited electronic state.[1] Dual fluorescence and phosphorescence emissions may, however, be observed if intersystem crossing (ISC) occurs at a competitive timescale to fluorescence and if the rate constant for phosphorescence emission is increased by a proximal heavy atom with a large spin–orbit coupling constant.[2–5] By capitalizing on this remote heavy-atom effect we and others have recently observed dual fluorescence and phosphorescence emissions at r.t. from metal complexes with a σ-bonded[6–11] or remotely attached bodipy (BDP) ligand.[12,13] Multiple emissions from a single compound can also result from inefficient Förster resonance energy transfer in dyads with two electronically decoupled, orthogonally aligned chromophores.[14] Intriguing examples are multiply emissive $Ir(ppy)_2(Q)$ complexes with two cyclometalated phenylpyridine (ppy) and a 2-hydroxyquinoline ligand Q, which show ligand-localized fluorescence from $^1n\pi^*$ and phosphorescence from ^{3}MLCT (MLCT = metal–ligand charge-transfer) states of the different ligands.[15] We report here on the new *meso*-Pt bodipy complex **BPtSPyr** (Scheme 1), which combines the above principles and presents four different emissions owing to the coexistence of energetically close-lying ligand-localized and charge-separated excited states.

[a]*Fachbereich Chemie, Universität Konstanz, Universitätsstraße 10, D-78457 Konstanz, Germany. E-mail: rainer.winter@uni-konstanz.de*
[b]*Department of Chemistry, University of Basel, St.-Johanns-Ring 19, CH-4056 Basel, Switzerland*

BPtSPyr was synthesized from *trans*-Pt(bodipy)I$(PEt_3)_2$ (**BPtI**)[7] by halogenide abstraction with AgOTf and subsequent addition to a solution of deprotonated 1-mercaptopyrene (pyrS). The same protocol was also used to prepare the complex **MesPtSPyr**, where the BDP chromophore is replaced by mesityl (Mes, Mes = 2,4,6-trimethylphenyl) from newly synthesized *trans*-PtBr(Mes)$(PEt_3)_2$ (for synthetic details and NMR spectroscopic characterization see ESI and Fig. S1–S18† therein).

The electronic absorption spectrum of **MesPtSPyr** is dominated by the ππ* band of the mercaptopyrene ligand at 431 nm (Fig. 1). Upon excitation into this band, **MesPtSPyr** exhibits dual fluorescence and phosphorescence emissions, at r.t. and at 77 K. Both emissions emanate from the mercaptopyrene ligand as follows from the typical shapes of the emissions and their lifetimes (Fig. S19–S25, ESI† and Table 1).[5,16,17] ISC in **MesPtSPyr** is obviously triggered by the heavy-metal effect of the attached Pt ion, similar to what has been observed in Pt complexes with a σ-bonded pyrenyl ligand.[5,16,17]

BPtSPyr reveals a three-band absorption pattern comprising of the structured pyrS-based ππ* band at 350–425 nm, the bodipy (BDP) ππ* absorption at 470 nm, and a partially overlapping, weaker pyrS-to-BDP charge-transfer (PB-CT) band at *ca.*

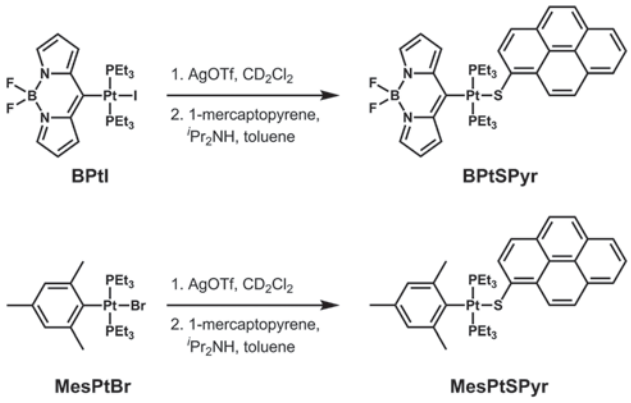

Scheme 1 Synthesis of **BPtSPyr** and **MesPtSPyr**.

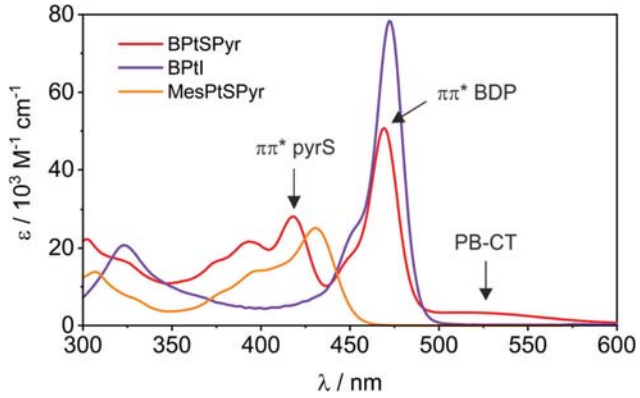

Fig. 1 UV/Vis spectra of **BPtSPyr**, **MesPtSPyr** and **BPtI** in toluene.

Table 1 Emission data of **MesPtSPyr** and **BPtSPyr**

Solvent	λ_{exc} [a]	λ_{fl} [b]	λ_{ph} [b] (assignment)	Φ_{ph} [c]	τ_{ph} [d]
MesPtSPyr					
Toluene	430	460[e]	664 (^{3}pyrS)	<0.01	448 ± 6 μs
Me-THF[f]	430	450	658 (^{3}pyrS)	n.d.	1.04 ± 0.06 ms
BPtSPyr					
Toluene	520		724 (^{3}PB-CT)	0.08	6.7 ± 0.4 μs
	470	484	724 (^{3}PB-CT)	0.15	6.7 ± 0.5 μs
	420		724 (^{3}PB-CT)	0.15	6.4 ± 0.3 μs
THF	520		784 (^{3}PB-CT)	n.d.	n.d.
	470	484[g]	635 (^{3}BDP)	n.d.	78.0 ± 0.4 μs,
			784 (^{3}PB-CT)		51.4 ± 0.8 ns
	420		784 (^{3}PB-CT)	n.d.	50.4 ± 0.3 ns
Acetone	520		861 (^{3}PB-CT)	n.d.	n.d.
	470	484	635 (^{3}BDP)	n.d.	49.9 ± 0.3 μs
			861 (^{3}PB-CT)		2.44 ± 0.02 ns
Me-THF[f]	530	n.o.	635 (^{3}BDP)	n.d.	279 ± 1 μs
	450		649 (^{3}pyrS)		1.12 ± 0.02 ms
	415				

[a] Excitation wavelength in nm. [b] Wavelength of the fluorescence (fl) or phophorescence (ph) emissions in nm. [c] Phosphorescence quantum yield. [d] Lifetime of the phosphorescence emissions. [e] τ_{fl} = 1.113 ± 0.005 ns, Φ_{ph} = 0.24. [f] Measured in a 2-MeTHF glass at 77 K. [g] τ_{fl} = 3.70 ± 0.2 ns.

500 nm. The latter has no equivalent in the precursors **BPtI** and **MesPtSPyr** (Fig. 1, Table S1, ESI†). The above band assignments are supported by time-dependent density functional theory (TD-DFT) calculations (Fig. S26, ESI†). According to our calculations all transitions are ligand-based with only minor Pt contributions to the corresponding donor and acceptor orbitals (Table S2†). In line with a CT character, the PB-CT excitation is solvatochromic while the pyrS and BDP ππ* absorptions are only modestly influenced by solvent polarity (Fig. S27, ESI†).

Importantly, and in contrast to **MesPtSPyr**, **BPtSPyr** exhibits four different emissions depending on excitation wavelength, solvent polarity and temperature (Fig. 2). As shown in Fig. 2a, excitation into the PB-CT absorption band at 520 nm leads to broad and unstructured NIR emission with a quantum yield of 8% in toluene. The emission shifts red with increasing solvent polarity, from 724 nm in toluene to 784 nm in THF and to 816 nm in acetone (Table 1). Its strong solvatochromism and the lifetime of

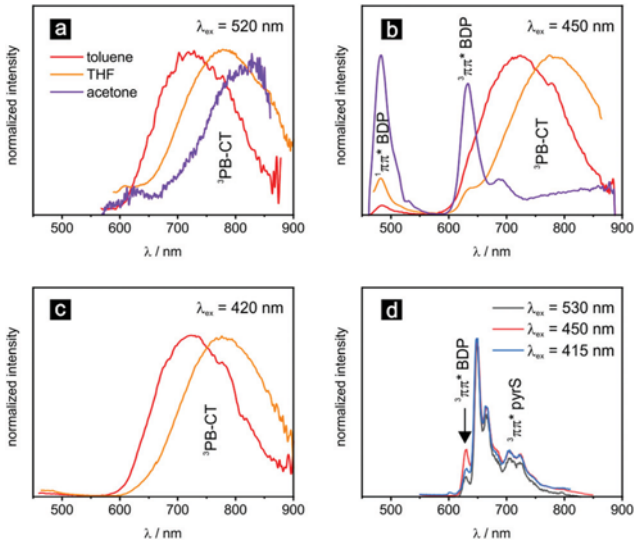

Fig. 2 Emission spectra of **BPtSPyr** in *ca.* 1 μM solutions of acetone, THF or toluene at r.t. on excitation at (a) 520 nm, (b) 450 nm and (c) 405 nm. (d) Emission spectra recorded in 2-MeTHF at 77 K at different excitation wavelengths.

6.7 μs in toluene (for lifetime decays see Fig. S28–S30, ESI†) indicate that this emission emanates from the ^{3}PB-CT state. We note that heavy atom-free donor-substituted BDPs were also shown to undergo efficient ISC to the T_1 state *via* an excited CT state; the latter systems are, however, non-phosphorescent.[18–20]

Excitation into the BDP ππ* absorption band at 470 nm (Fig. 2b and S31, ESI†) opens two further radiative pathways: BDP-based fluorescence at 484 nm and phosphorescence at 635 nm are observed in addition to the ^{3}PB-CT emission. Changing the solvent from toluene to THF or acetone increases the energy separation between the BDP ^{3}ππ* and the ^{3}PB-CT states and allows for tuning of the emission colour from red in toluene (CIE coordinates 0.6052/0.3211 in toluene) to almost white in THF (CIE coordinates: 0.2209/0.3206) or acetone (CIE coordinates 0.3357/0.2901). Concomitantly with its red-shift, the lifetime of the ^{3}PB-CT emission decreases from 6.7 μs in toluene solution to only 2.4 ns in acetone (Fig. S30a, ESI†). This in turn increases the intensity ratio of the ^{1}ππ*/^{3}ππ* to the ^{3}PB-CT emissions (Fig. 2b). We note that the BDP-based emissions of **BPtSPyr** are not due to contamination with the **BPtI** precursor (Fig. S32, ESI†). Triple emission upon excitation into the BDP ππ* band at 470 nm indicates that ISC from the ^{1}ππ* to the ^{3}ππ* state of the BDP ligand as well as formation of the ^{1}PB-CT state and subsequent ISC to the ^{3}PB-CT state occur at similar rates as fluorescence from the BDP ^{1}ππ* state. When the sample is excited into the pyrS ππ* band at 415 nm, again solely ^{3}PB-CT emission is observed, but with an even increased quantum yield of 15% (λ_{exc} = 420 nm) as compared to 8% for λ_{exc} = 520 nm (Fig. 2a and c), rendering **BPtSPyr** a powerful NIR emitter. All the above conclusions are fully supported by excitation *vs.* emission maps and excitation spectra (Fig. S33 and S34, ESI†).

Emission spectra recorded in a glassy Me-THF matrix at 77 K show only two features, irrespective of the excitation wave-

length: the $^3\pi\pi^*$ BDP emission with a maximum at 635 nm and a typical lifetime of 279 μs (Fig. S35, ESI†) as well as a structured emission enveloping the region in from 649 to 750 nm (Fig. 2d). This latter feature and its lifetime of 1.12 ms (Fig. S35, ESI†) are typical of a pyrene-based $^3\pi\pi^*$ emission.[5,16,17] The $^3\pi\pi^*$ excited states of the BDP and pyrS ligands are hence both accessible from excitation into any band in the rigid matrix. This indicates that, at 77 K, population of the close-lying BDP and pyrS $^3\pi\pi^*$ from the ^{1}PB-CT state of **BPtSPyr** is more rapid than direct intersystem crossing to the ^{3}PB-CT state and that deactivation to the ^{3}PB-CT state is blocked under these conditions. One possible explanation is that the ^{1}PB-CT and ^{3}PB-CT states possess very similar nuclear coordinates and the BDP and pyrS $^3\pi\pi^*$ potential wells have more easily accessible intersections with the ^{1}PB-CT potential well. Previous studies have similarly demonstrated direct singlet-to-triplet electron-transfer by spin–orbit coupling.[21–23]

The Jablonski diagram of Scheme 2 summarizes the processes following the different excitations of **BPtSPyr**. Electronic decoupling of the pyrS- and the BDP-localized $^1\pi\pi^*$ states, as indicated by the confinement of the HOMO to the pyrS and of the LUMO to the BDP ligand (Fig. S26, ESI†), explains the absence of pyrS to BDP energy transfer from the pyrene-based $^1\pi\pi^*$ state S_3 and of any BDP emission after excitation into the pyrS ππ* band at 415 nm. The BDP-based $^1\pi\pi^*$ and $^3\pi\pi^*$ states S_2 and T_3 are thus exclusively populated by excitation into the BDP $^1\pi\pi^*$ band. In contrast, the ^{3}PB-CT state, which constitutes the energetically lowest excited triplet state T_1, is accessible from all three excited singlet states, either *via* IC to the ^{1}PB-CT and subsequent ISC, or *via* ISC and subsequent electron transfer from the higher-lying pyrS-based T_2 and BDP-based T_3 states (note that **MesPtSPyr** also undergoes ISC from the pyrene-based $^1\pi\pi^*$ state). At 77 K, direct singlet to triplet electron-transfer from the ^{1}PB-CT state allows population of the pyrS- and BDP-based triplet states T_2 and T_3 (blue arrows in Scheme 2) and renders the pyrS-based phosphorescence emission observable, which, at r.t., is quenched by rapid decay into the lower-lying ^{3}PB-CT state.

The proposed excited state cascade is further supported by transient absorption (TA) spectroscopy in THF. TA spectra recorded over the first 200 ns after excitation are very similar to each other, irrespective of whether the sample is excited at 410

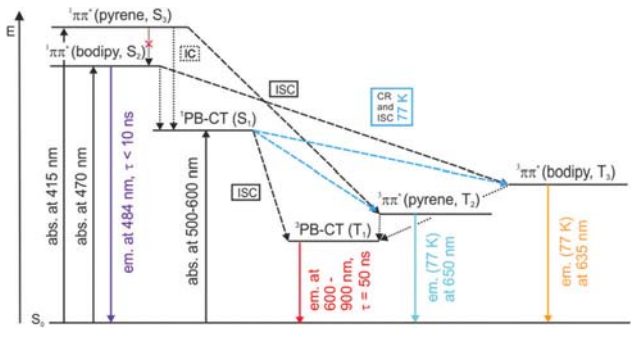

Scheme 2 Qualitative Jablonski diagram.

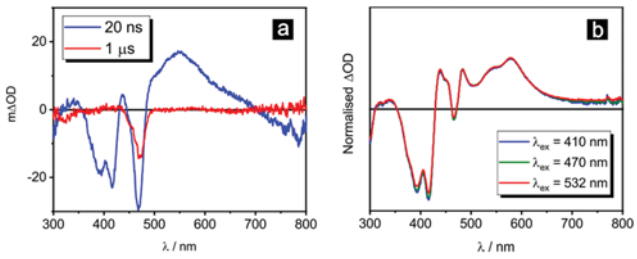

Fig. 3 Transient absorption spectra of **BPtSPyr** at r.t. (a) in deaerated 20 μM THF solution at different time delays after excitation at 470 nm; and (b) in a 20 μM toluene solution directly after laser excitation at the given wavelength. All spectra are time-integrated over 200 ns.

(pyrS), 470 (BDP), or 532 nm (PB-CT absorption) (Fig. 3 and Fig. S36, ESI†). Three main features are observed: the bleached pyrS and BDP ground state absorption signals at *ca.* 400 nm or 470 nm, and an excited state absorption (ESA) signal at 550 nm, which we assign to the $pyrS^{\bullet+}$ radical cation (*vide infra*). Identical monoexponential kinetics with a common time constant of 50 ns were found for all three transients when excited at 532 nm (for single point kinetics for each TA feature see Fig. S37 and S38, ESI†). When excited into the BDP absorption at 470 nm the features at 415 nm and 550 nm still have a time constant of 50 ns, but the bleach recovery at 475 nm has much longer kinetics of 16.5 μs in THF. This is in accordance with the long-lived BDP $^3\pi\pi^*$ excited state in that solvent (red trace in Fig. S37a, ESI†). Transient absorption bleach recoveries and decays match the luminescence lifetimes in all cases. This corroborates that none of the observable emissions originate from impurities but represent inherent photoluminescence from **BPtSPyr**.

The common CT state after excitation should exhibit spectroscopic features similar to the oxidized and reduced forms of **BPtSPyr**. Cyclic voltammograms show a reversible oxidation at +0.18 V and a reduction at −1.97 V against the ferrocene/ferrocenium couple (Fig. S39 and Table S3, ESI†). This allowed us to experimentally probe the UV/Vis/NIR features of the oxidized and reduced forms of **BPtSPyr** by means of spectroelectrochemistry. Upon oxidation, the pyrS-based ππ* absorption band bleaches while the BDP ππ* band exhibits an only minor red-shift of 316 cm^{-1} (Fig. 4). Based on literature data[24,25] and the results of our TD-DFT calculations (Fig. S40 and Table S4, ESI†), the new absorption bands at *ca.* 520, 550, 750, and 1000 nm can be assigned to ππ* transitions of the $pyrS^{\bullet+}$ radical cation. When **BPtSPyr** is reduced, the BDP ππ* and the PB-CT absorption bands bleach while the pyrS-based ππ* band experiences a moderate red-shift. The weak new band at 518 nm constitutes mainly a ππ* transition of the reduced BDP ligand (Fig. S41 and S42, Table S5, ESI†); it is essentially identical in shape and energy to that observed for $\mathbf{BPtI}^{\bullet-}$.[9] Calculated spin densities for the **BPtSPyr** radical cation and anion also agree with a pyrS-based oxidation and a BDP-based reduction (Fig. 5 and Table S6, ESI†). The results of our spectroelectrochemical experiments and our calculations thus confirm our assignment of the ESA signal to the $pyrS^{\bullet+}$ constituent as well as the character of the HOMO and LUMO of **BPtSPyr**.

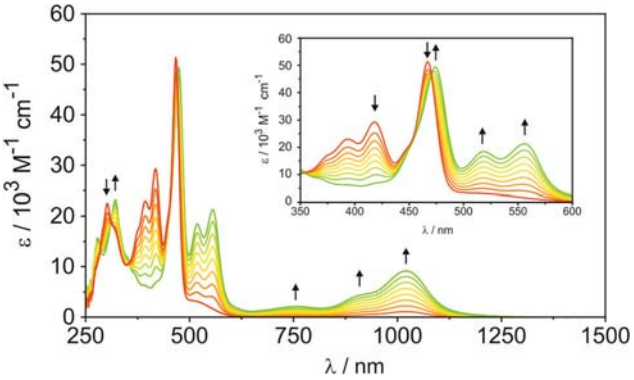

Fig. 4 Changes of UV/Vis/NIR spectra of **BPtSPyr** on oxidation (THF, NBu_4PF_6, 293 K).

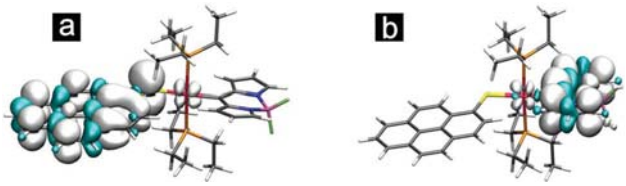

Fig. 5 Calculated spin densities of (a) the radical cation and (b) the radical anion of **BPtSPyr**.

In summary, the **BPtSPyr** dyad combines several remarkable features. It constitutes an extremely rare case of a compound showing emissions from four different excited states and acts as a powerful NIR emitter. Its emission profiles and colour can be tuned by the excitation wavelength and solvent polarity from deep red to almost white. The crucial role of the $pyrS^{\bullet+}$–Pt-$BDP^{\bullet-}$ charge-transfer state within the excited state cascade was identified by TA spectroscopy, spectroelectrochemical methods and TD-DFT calculations.

Conflicts of interest

The authors declare no competing financial interests.

Acknowledgements

This work was supported by Deutsche Forschungsgemeinschaft (grant Wi1262/10-2) and the Swiss National Science Foundation (grant number 200021_176780).

Notes and references

1 M. Kasha, *Discuss. Faraday Soc.*, 1950, **9**, 14–19.
2 C.-W. Hsu, C.-C. Lin, M.-W. Chung, Y. Chi, G.-H. Lee, P.-T. Chou, C.-H. Chang and P.-Y. Chen, *J. Am. Chem. Soc.*, 2011, **133**, 12085–12099.
3 C.-C. Hsu, C.-C. Lin, P.-T. Chou, C.-H. Lai, C.-W. Hsu, C.-H. Lin and Y. Chi, *J. Am. Chem. Soc.*, 2012, **134**, 7715–7724.
4 Y.-C. Chang, K.-C. Tang, H.-A. Pan, S.-H. Liu, I. O. Koshevoy, A. J. Karttunen, W.-Y. Hung, M.-H. Cheng and P.-T. Chou, *J. Phys. Chem. C*, 2013, **117**, 9623–9632.
5 W. Y. Heng, J. Hu and J. H. K. Yip, *Organometallics*, 2007, **26**, 6760–6768.
6 F. Geist, A. Jackel and R. F. Winter, *Inorg. Chem.*, 2015, **54**, 10946–10957.
7 P. Irmler and R. F. Winter, *Dalton Trans.*, 2016, **45**, 10420–10434.
8 F. Geist, A. Jackel, P. Irmler, M. Linseis, S. Malzkuhn, M. Kuss-Petermann, O. S. Wenger and R. F. Winter, *Inorg. Chem.*, 2017, **56**, 914–930.
9 P. Irmler and R. F. Winter, *Organometallics*, 2018, **37**, 235–253.
10 W. Wu, J. Zhao, H. Guo, J. Sun, S. Ji and Z. Wang, *Chem. – Eur. J.*, 2012, **18**, 1961–1968.
11 F. Zhong, A. Karatay, L. Zhao, J. Zhao, C. He, C. Zhang, H. G. Yaglioglu, A. Elmali, B. Küçüköz and M. Hayvali, *Inorg. Chem.*, 2015, **54**, 7803–7817.
12 J. Sun, F. Zhong, X. Yi and J. Zhao, *Inorg. Chem.*, 2013, **52**, 6299–6310.
13 W. Wu, J. Sun, X. Cui and J. Zhao, *J. Mater. Chem. C*, 2013, **1**, 4577–4589.
14 B. Ma, P. I. Djurovich, M. Yousufuddin, R. Bau and M. E. Thompson, *J. Phys. Chem. C*, 2008, **112**, 8022–8031.
15 T. Tsuboi, D.-F. Huang, T. J. Chow and W. Huang, *Opt. Mater.*, 2014, **36**, 1734–1738.
16 J. Hu, J. H. K. Yip, D.-L. Ma, K.-Y. Wong and W.-H. Chung, *Organometallics*, 2009, **28**, 51–59.
17 W. Wu, W. Wu, S. Ji, H. Guo and J. Zhao, *Eur. J. Inorg. Chem.*, 2010, **2010**, 4470–4482.
18 M. A. Filatov, S. Karuthedath, P. M. Polestshuk, S. Callaghan, K. J. Flanagan, M. Telitchko, T. Wiesner, F. Laquai and M. O. Senge, *Phys. Chem. Chem. Phys.*, 2018, **20**, 8016–8031.
19 X.-F. Zhang and N. Feng, *Chem. – Asian J.*, 2017, **12**, 2447–2456.
20 S. Ji, J. Ge, D. Escudero, Z. Wang, J. Zhao and D. Jacquemin, *J. Org. Chem.*, 2015, **80**, 5958–5963.
21 M. R. Wasielewski, D. G. Johnson, W. A. Svec, K. M. Kersey and D. W. Minsek, *J. Am. Chem. Soc.*, 1988, **110**, 7219–7221.
22 S.-H. Lee, A. G. Larsen, K. Ohkubo, Z.-L. Cai, J. R. Reimers, S. Fukuzumi and M. J. Crossley, *Chem. Sci.*, 2012, **3**, 257–269.
23 T. Higashino, T. Yamada, M. Yamamoto, A. Furube, N. V. Tkachenko, T. Miura, Y. Kobori, R. Jono, K. Yamashita and H. Imahori, *Angew. Chem., Int. Ed.*, 2016, **55**, 629–633.
24 T. Shida and S. Iwata, *J. Am. Chem. Soc.*, 1973, **95**, 3473–3483.
25 J. Maurer, M. Linseis, B. Sarkar, B. Schwederski, M. Niemeyer, W. Kaim, S. Záliš, C. Anson, M. Zabel and R. F. Winter, *J. Am. Chem. Soc.*, 2008, **130**, 259–268.